ACS APPLIED MATERIALS & INTERFACES

Research Article

www.acsami.org

Co-intercalation of Acid Red 337 and a UV Absorbent into Layered Double Hydroxides: Enhancement of Photostability

Dianqing Li, Leilei Qian, Yongjun Feng, Junting Feng, Pinggui Tang,* and Lan Yang*

State Key Laboratory of Chemical Resource Engineering, Beijing University of Chemical Technology, Beijing 100029, People's Republic of China

Supporting Information

ABSTRACT: Organic–inorganic hybrid pigments with enhanced thermo- and photostability have been prepared by co-intercalating C.I. Acid Red 337 (AR337) and a UV absorbent (BP-4) into the interlayer of ZnAl layered double hydroxides through a coprecipitation method. The obtained compounds were characterized by X-ray diffraction, Fourier transform infrared spectroscopy, scanning electron microscopy, thermogravimetric–differential thermogravimetric–differential thermal analysis, UV–visible spectroscopy, and the International Commission on Illumination (CIE) 1976 L*a*b* color scales. The results show the successful co-intercalation of AR337 and BP-4 into the interlayer region of layered double hydroxides (LDHs) and reveal the presence of host–guest interactions between LDH host layers and guest anions of AR337 and BP-4 and guest–guest interactions between AR337 and BP-4. The intercalation can improve the thermostability of AR337 due to the protection of LDH layers. Moreover, the co-intercalation of AR337 and BP-4 not only markedly enhances the photostability of AR337 but also significantly influences the color of the hybrid pigment.

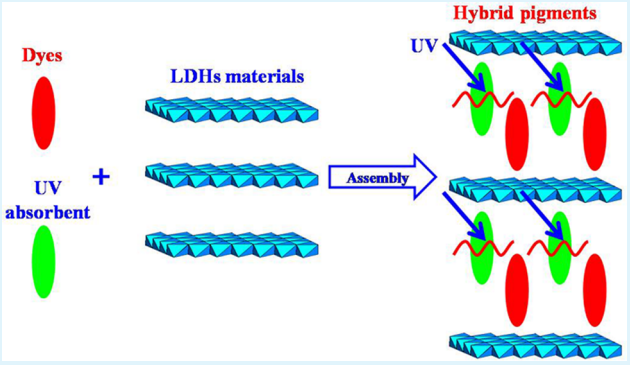

KEYWORDS: *layered double hydroxides, hybrid pigment, intercalation, thermostability, photostability*

1. INTRODUCTION

Organic pigments are widely used in the area of paints, printing inks, coatings, and plastics because they have many advantages such as light tones, various species, wide color gamut, high color strength, brilliance, and so on.[1,2] However, the poor thermo- and photostability of the organic pigments seriously limit their use in the fields of plastics and coatings, as they would undergo thermal decomposition when the plastics are processed at higher temperatures, and they would lose their bright color when the coatings are used under sunlight for a certain time.[3] Therefore, it is necessary to find ways to improve the performance of the organic pigments, especially their thermo- and photostability. Recently, organic–inorganic hybrid materials have received a great deal of interest because they have merits of both organic and inorganic parts. The organic parts can offer flexibility, versatility, and functionality, and the inorganic parts can provide high thermal and mechanical resistance.[4] Thus, it is possible to improve the thermo- and photostability of organic chromophores by making sandwich structures with inorganic matrixes.

Layered double hydroxides (LDHs), a class of anionic layered clays, have a general formula of $[M_{1-x}^{2+}M_x^{3+}(OH)_2]^{x+}(A^{n-})_{x/n}\cdot mH_2O$, where x usually ranges from 0.2 to 0.33; M^{2+} and M^{3+} represent various di- and trivalent metal cations in the LDH host sheets; and A^{n-} is the interlayer guest anion.[5,6] LDHs are composed of positively charged host metal hydroxide layers and negatively charged guest anions through weak interactions. They have received much attention in the last 20 years due to their adjustable chemical composition, tunable charge density, anion exchange ability, and good thermal stability.[7,8] Because of their multifunctionalities, LDHs have been widely used in the areas of catalysis,[9−11] biochemistry,[12,13] adsorption,[14−16] anion exchange,[17] sensors,[18,19] polymer additives,[7,20−22] and so on.

Recently, considerable attention has been focused on the fabrication of organic chromophore anions intercalated LDHs, which show novel functionalities that are not present in the pristine organic chromophores.[23−26] For example, Evans blue,[27] Niagara blue 3B,[28] *N*,*N*′-di(phenyl-3,5-disulfonic acid)perylene-3,4,9,10-tetracarboxydiimide,[25] and *N*,*N*′-bis(4-benzosulfonic acid)-perylene-3,4,9,10-tetracarboxylbisimide[26] have been successfully intercalated into the interlayer room of the LDHs, and it was found that the intercalation can improve the photostability of the dyes. Lately, we have successfully intercalated Mordant Yellow 3 (MY3) anions into the interlayer space of ZnAl–LDHs by a coprecipitation method and found that the thermo- and photostability of MY3 anions had been improved due to the host–guest interactions.[29] Though the photostability

Received: March 23, 2014
Accepted: November 18, 2014
Published: November 18, 2014

of the organic chromophore can be improved to a certain degree by intercalation into the interlayer room of LDHs, the organic chromophore still suffers from photo degradation. As a result, the color of the hybrid pigments will fade after being used several times. Hence, there is still a need to improve the photostability of these hybrid pigments.

Herein, we report a strategy to improve the photostability of the organic chromophore−LDH hybrid pigments. Acid red 337 (AR337) is a kind of azo dye which is widely used in dyeing nylon fabric due to its bright color. Its structural formula is shown in Figure 1a. Though the thermal stability of AR337 is

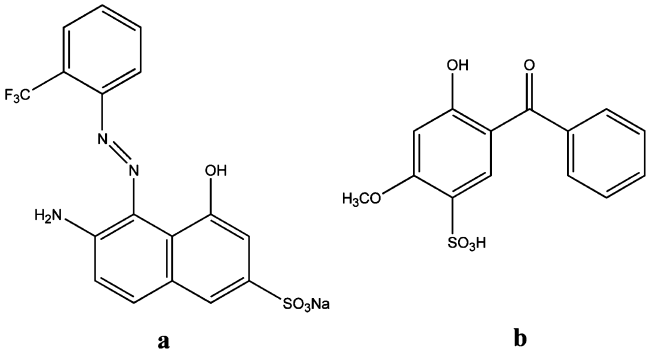

Figure 1. Structural formulas of (a) AR337 and (b) BP-4.

excellent, its photostability is poor, which severely limits its application range. In this work, AR337 has been co-intercalated into the interlayer spacing of ZnAl−LDHs with a UV absorbent, 2-hydroxy-4-methoxy-5-sulfonic acid diphenylketone (BP-4, Figure 1b, its sodium salt is denoted as NaBP-4), to fabricate organic−inorganic hybrid pigments with high photostability. The incorporation of BP-4 can not only tune the color of the hybrid pigments but also significantly improve the photostability of the pigments.

2. EXPERIMENTAL SECTION

2.1. Materials. NaOH, $Zn(NO_3)_2{\cdot}6H_2O$, $Al(NO_3)_3{\cdot}9H_2O$, sodium dodecyl benzenesulfonate (SDBS), sodium dodecyl sulfonate (SDS), anhydrous ethanol, and ethylene glycol were analytical-grade reagents and used as received without any further purification. Deionized water with an electrical conductivity of less than 10^{-6} S cm^{-1} was decarbonated before use in all synthesis and washing processes. Acid red 337 was a commercial product with a purity of 94% and recrystallized three times in water before use. BP-4 was a commercial product with a purity of 99% and used as received without any further purification.

2.2. Preparation of ZnAl−NO_3−LDH. ZnAl−NO_3−LDH was prepared by the coprecipitation method. $Zn(NO_3)_2{\cdot}6H_2O$ (0.015 mol) and $Al(NO_3)_3{\cdot}9H_2O$ (0.005 mol) were dissolved in 50 mL of water to form a mixed salt solution. NaOH (0.04 mol) was dissolved in water (50 mL) to form an alkali solution and then added dropwise to the salt solution with vigorous stirring under N_2 atmosphere. The resulting slurry was then aged at 95 °C for 6 h under a N_2 stream. The product cake was collected after eight repetitive centrifugation and dispersion cycles in deionized water, and part of the cake was dried at 100 °C for 12 h for characterization.

2.3. Preparation of ZnAl−AB−LDHs. AR337 and BP-4 anions co-intercalated LDHs (ZnAl−AB−LDHs) were synthesized through coprecipitation method. A mixture of BP-4, NaOH, and AR337 was dissolved in ethylene glycol (40 mL) by vigorous stirring under N_2 atmosphere at 50 °C in a water bath. The total molar amounts of AR337 and BP-4 were fixed to be 3.0 mmol, where the molar percentage of AR337 was set to be 0, 20, 40, 60, 80, 100%, respectively, and the molar ratio of NaOH/BP-4 is 1. $Zn(NO_3)_2{\cdot}6H_2O$ (7.5 mmol) and $Al(NO_3)_3{\cdot}9H_2O$ (2.5 mmol) were dissolved in water (30 mL) and then added into the above ethylene glycol solution. NaOH (17 mmol) was dissolved in water (30 mL) and then added dropwise into the mixed solution with vigorous stirring under N_2 atmosphere. The resulting slurry was then aged at 95 °C with violent agitation under a N_2 stream for 6 h. The product cake was collected after eight repetitive centrifugation and dispersion cycles in hot deionized water and three cycles in ethanol. Finally, the obtained product was dried at 100 °C in an oven for 12 h. The obtained LDHs were denoted as LDH-*n*, where *n* represents the molar percentage of AR337.

AR337 and SDBS anions co-intercalated LDH (ZnAl−AS−LDH), and AR337 and SDS co-intercalated LDH (ZnAl−ASS−LDH) with 20% molar percentage of AR337 were also synthesized through above process for comparison.

The physical mixture of ZnAl−NO_3−LDH and AR337 (PM) was obtained by vigorous stirring the obtained ZnAl−NO_3−LDH cake and AR337 in water until a uniform mixture formed, centrifuged, washed with ethanol three times, and dried at 100 °C for 12 h. The weight percentage of AR337 in PM is equal to that of LDH-20.

2.4. Photostability Evaluation. To eliminate the influence of the contents of the dyes on the evaluation of the photostability of the samples, we utilized samples with the same AR337 content for testing. The cakes of LDH-40, LDH-60, LDH-80, and LDH-100 after eight repetitive centrifugation and dispersion cycles in hot deionized water were uniformly mixed and diluted with ZnAl−NO_3−LDH cake by vigorous stirring, respectively, to obtain a mixture where the weight percentage of AR337 is same as that of LDH-20. The mixtures were collected and denoted as MLDH-40, MLDH-60, MLDH-80, and MLDH-100, respectively, after being washed with ethanol three times and dried at 100 °C for 12 h. The photostability of the samples were tested in a UV-accelerated photoaging instrument (with a high-pressure mercury−ultraviolet lamp as a UV light source, 1000 W power, and λ_{max} = 360 nm). The color difference (ΔE) value and the absorption in the diffuse reflectance spectra was recorded after each UV irradiation for 5 min, and each sample was irradiated for a total of 50 min.

2.5. Characterization. X-ray diffraction (XRD) patterns were collected on a Shimadzu XRD−6000 diffractometer with monochromatic Cu Kα radiation (λ = 0.154 nm) operating at 40 kV and 30 mA. FT−IR spectra were recorded on a Bruker Vector 22 infrared spectrophotometer with 2 cm^{-1} resolution using the KBr disk method with a mass ratio of sample/KBr of 1:100 for AR337 and BP-4, and 3:100 for LDHs. The morphology was investigated by means of a scanning electron microscope (SEM, Hitachi S−3500N) operating at 20 kV. Thermogravimetric−differential thermogravimetric−differential thermal analysis (TG−DTG−DTA) were performed on a PCT−IA instrument in the temperature range of 25−800 °C with a heating rate of 10 °C min^{-1} under air atmosphere. Elemental analyses for Zn and Al of the ZnAl−AB−LDHs were performed on an ICPS-7500 type inductively coupled plasma emission spectrometer (ICP−ES). Carbon and nitrogen analyses were conducted on Elementar Vario EL Cube elemental analyzer. The digital photos of the samples were taken with a digital camera. The UV−vis absorption spectra were recorded on a Shimadzu UV−2501PC spectrometer, and an integrating sphere was equipped to the spectrometer to measure the diffuse reflectance spectra of powdered samples. The L*a*b* values and color difference (ΔE) values of samples aged under UV light were determined in terms of the International Commission on Illumination (CIE) 1976 L*a*b* color scales using a TC-P2A automatic colorimeter (Xinao Yike Optic−Electronic Co., Beijing) after it was calibrated with a standard black cylinder and a white $BaSO_4$ plate.

3. RESULTS AND DISCUSSION

3.1. Structure and Morphology of the Prepared LDHs. Figure 2 shows the powder XRD patterns of ZnAl−NO_3−LDH, ZnAl−AB−LDHs, and ZnAl−AS−LDH. It is clear that all samples are defined by a series of typical (00*l*) (l = 3, 6, 9) Bragg reflections. The typical (003) reflection of ZnAl−NO_3−

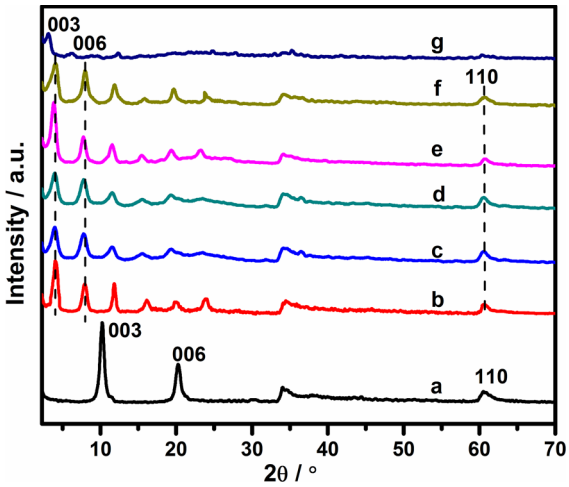

Figure 2. XRD patterns of (a) ZnAl–NO_3–LDH, (b) LDH-20, (c) LDH-40, (d) LDH-60, (e) LDH-80, (f) LDH-100, and (g) ZnAl–AS–LDH.

LDH (Figure 2a) appears at 2θ = 10.24°, corresponding to a basal spacing of 0.86 nm, which is in agreement with the literature.[30] For AR337 and BP-4 co-intercalated LDHs, the (003) reflections appear at about 2θ = 3.98°, and the corresponding basal spacing values are about 2.22 nm, suggesting that AR337 and BP-4 anions have been successfully co-intercalated into the interlayer galleries of ZnAl–LDHs and formed only one crystal phase. The (003) reflection of ZnAl–AS–LDH (Figure 2g) appears at 2θ = 3.12°, which corresponds to a basal spacing of 2.83 nm, indicating the successful co-intercalation of AR337 and SDBS anions into the interlayer galleries of LDHs and the formation of only one crystal phase.

It has been revealed that the guest anions in the interlayer galleries of LDHs can interact with each other through $\pi-\pi$ interactions between the benzene rings and form H-type or J-type aggregates.[26,28,31] Therefore, the arrangement of anions in the interlayer of LDH mainly depends on the gallery height, the size and structure of anions, and $\pi-\pi$ interactions between the interlayer anions. When the gallery height and anions are given, the $\pi-\pi$ interactions will play a key role in the arrangement of anions, and the neighboring anions would adopt an arrangement with the benzene rings highly overlap with each other. By subtraction of the layer thickness of 0.48 nm, the gallery height is about 1.74 nm for each ZnAl–AB–LDH. The length of AR337 and BP-4 anions estimated from the distance between the sulfonate group and the hydrogen atom is 1.194 and 0.956 nm, respectively. Taking $\pi-\pi$ interaction, gallery height, and the length of AR337 anion into account, AR337 anions would form a monolayer with interdigitated arrangement, and form J-type aggregates in the channel of LDH-100 (Figure 3A), which was confirmed by its UV–vis spectrum as discussed in the UV–vis spectra section. Hence, the benzene ring in the tailor side of one AR337 anion will highly overlap with the benzene ring in the head side of the neighboring AR337 anion. Because the distance between the sulfonate groups of the two neighboring AR337 anions that form the J-type aggregate is about 1.92 nm, the J-type aggregate would be tilted at an angle of about 25° to the LDH layers, which also means that AR337 anions are tilted at an angle of about 25° to the LDH layers in favor of the highly overlap of the benzene rings. Because the size of BP-4 is much smaller than that of AR337, the arrangement of AR337 in

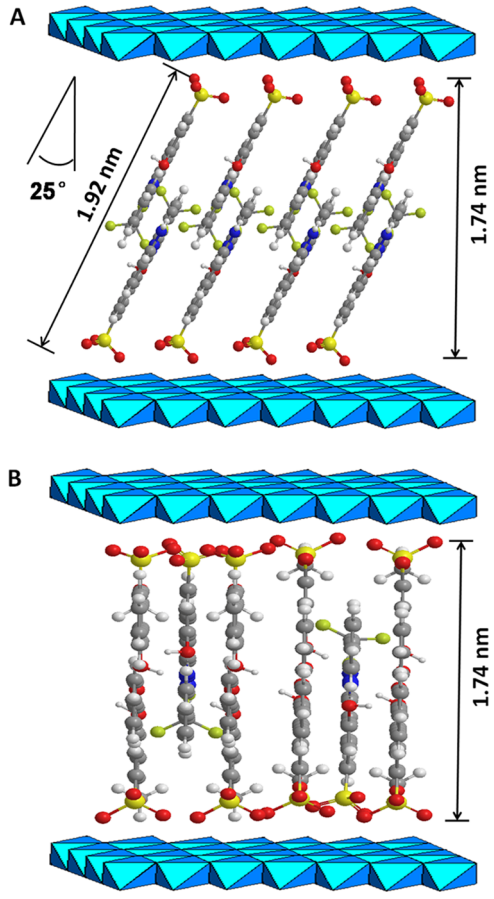

Figure 3. Models of the possible arrangements of the anions in the interlayer of (A) LDH-100 and (B) LDH-20.

the interbed of LDH-20 will be different from that of LDH-100. Considering the gallery height and the length of the AR337 and BP-4 anions, AR337 and BP-4 anions in the channel of LDH-20 (Figure 3B) would adopt an interdigitated arrangement perpendicular to the LDHs layers in favor of the highly overlap of the benzene rings of AR337 and BP-4 anions (each AR337 anion was surrounded by four BP-4 anions). Both oblique and perpendicular arrangements may exist in the interlayer of LDH-40, LDH-60, and LDH-80 for AR337 anions.

The FT–IR spectra of AR337, BP-4, SDBS, ZnAl–AB–LDHs and ZnAl–AS–LDH are illustrated in Figure 4. In the spectrum of AR337 (Figure 4a), the absorption bands at 1612 and 1587 cm^{-1} correspond to the skeletal vibration of phenyl groups, and the bands at 1175 and 1054 cm^{-1} can be ascribed to the antisymmetric and symmetric stretching vibrations of $-SO_3^-$ groups, respectively.[26] The FT–IR spectra of ZnAl–AB–LDHs (Figure 4d–g) reveal both the characteristic features of LDH-like materials and interlayer anions. The broad absorption bands centered at about 3450 cm^{-1} can be assigned to the stretching vibration of the hydroxyl groups of LDH layers and interlayer water molecules,[29,32] and the band at 425 cm^{-1} can be ascribed to O–M–O vibration in the LDH layers.[33] After intercalation, the symmetric stretching vibrations of $-SO_3^-$ groups of AR337 shift from 1054 to 1050 cm^{-1}, suggesting that the host–guest interactions between the ZnAl–LDHs layers and interlayer anions are different from those between AR337 anions and sodium ions in the dye salts.[27,34] The spectrum of ZnAl–AS–LDH shows the characteristic absorption bands of the LDH layers and the AR337 and SDBS

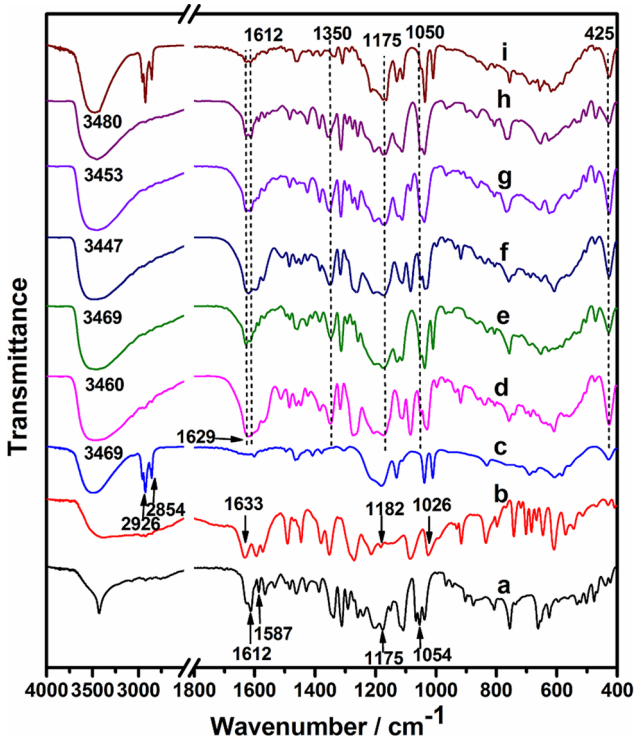

Figure 4. FT−IR spectra of (a) AR337, (b) BP-4, (c) SDBS, (d) LDH-20, (e) LDH-40, (f) LDH-60, (g) LDH-80, (h) LDH-100, and (i) ZnAl−AS−LDH.

anions, suggesting that AR337 and SDBS have been co-intercalated into the interlayer room of ZnAl−LDH. There is no absorption band at about 1360 cm^{-1} ascribed to CO_3^{2-} anions, indicating that there are no CO_3^{2-} anions in the interlayer of ZnAl−AS−LDH. As the preparation procedures for all the LDHs are the same, no CO_3^{2-} anions would be intercalated into the interlayer of ZnAl−AB−LDHs. Hence, the absorption peaks at about 1350 cm^{-1} for ZnAl−AB−LDHs are assigned to AR337 and BP-4 anions. These results, together with the XRD analysis, confirm the formation of a new kind of organic−inorganic hybrid pigment ZnAl−AB−LDHs.

Figure 5 displays the SEM images of ZnAl−AB−LDHs obtained by a scanning electron microscope. The micrographs show that the prepared samples present typical platelet-like, irregularly shaped morphology.

3.2. Chemical Composition Analysis. The chemical compositions of ZnAl−AB−LDHs are listed in Table 1. The results confirm that AR337 and BP-4 anions have been co-intercalated into the interlayer of the LDHs. The Zn/Al and N/Al molar ratios are calculated according to their weight contents in Table 1. The amounts of interlayer water are calculated based on the mass loss from 100 to 200 °C in the TG curves of ZnAl−AB−LDHs. The molar contents of AR337 and BP-4 anions are calculated based on the N/Al molar ratio and charge balance. The molar percents of AR337 in the interlayer of ZnAl−AB−LDHs are close to the feed ratios, indicating that the contents of AR337 in the interlamellar room of LDHs can be tuned according to the demand.

3.3. TG−DTG−DTA Analysis. The thermal stability of the hybrid pigments were investigated by TG−DTG−DTA analysis. Figure 6 displays the TG−DTG−DTA curves of AR337, LDH-0, LDH-20, and LDH-100. Two mass loss steps are observed in the TG curve of AR337 (Figure 6a) along with three mass loss peaks in its DTG curve and three exothermic peaks centered at 361, 494, and 567 °C in its DTA curve. The first loss step with a mass loss of 14.3% from 330 to 377 °C can be attributed to the oxidative thermal decomposition of AR337, and the second mass loss region with a loss of 72.1% in the temperature range of 377−800 °C can be assigned to the further decomposition of the residue.

There are three mass loss steps in the TG curve of LDH-0 (Figure 6b). The first mass loss step from 50 to 210 °C with a mass loss of 6.4% is assigned to the loss of adsorbed water and the removal of interlayer water. The second mass loss step, which shows a mass loss of 7.4% from 210 to 300 °C, is due to the dehydroxylation of the LDH layers.[35] The third mass loss step is in the range of 300−800 °C, and the exothermic peak at 463 °C indicates the oxidative thermal decomposition of BP-4

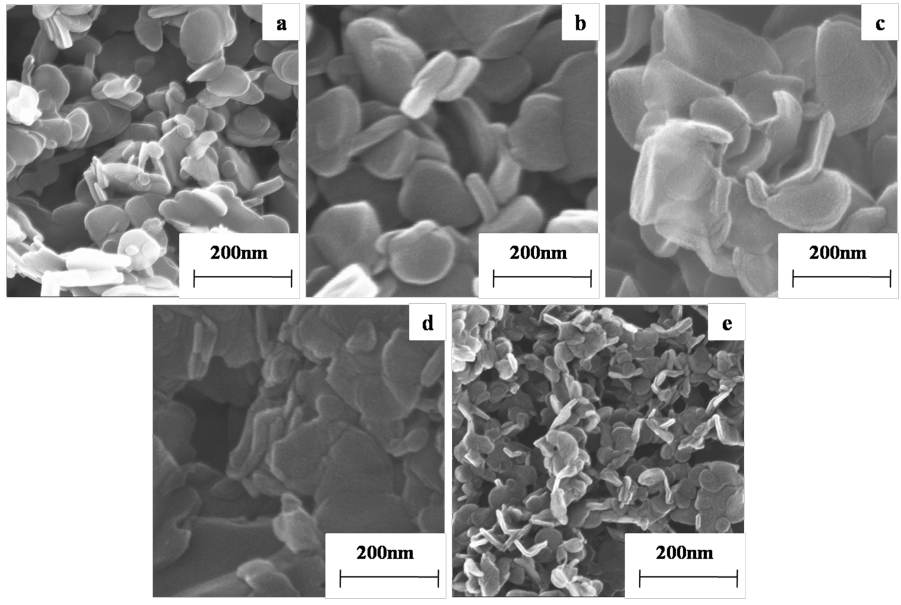

Figure 5. SEM images of (a) LDH-20, (b) LDH-40, (c) LDH-60, (d) LDH-80, and (e) LDH-100.

Table 1. Chemical Compositions (wt%) and Structural Formulas of ZnAl−AB−LDHs

samples	Zn	Al	N	C	Zn/Al molar ratio	AR337 molar percent	structural formulas
LDH-0	24.39	3.83		26.31	2.628	0	$Zn_{0.724}Al_{0.276}(OH)_2(BP\text{-}4)_{0.276}\cdot 0.43H_2O$
LDH-20	26.06	4.15	1.356	26.13	2.592	21	$Zn_{0.722}Al_{0.278}(OH)_2(AR337)_{0.058}(BP\text{-}4)_{0.22}\cdot 0.64H_2O$
LDH-40	24.23	3.93	2.296	26.59	2.545	38	$Zn_{0.718}Al_{0.282}(OH)_2(AR337)_{0.106}(BP\text{-}4)_{0.176}\cdot 0.59H_2O$
LDH-60	25.01	4.04	3.359	27.08	2.556	54	$Zn_{0.719}Al_{0.281}(OH)_2(AR337)_{0.15}(BP\text{-}4)_{0.131}\cdot 0.63H_2O$
LDH-80	25.39	3.83	4.368	27.19	2.737	78	$Zn_{0.732}Al_{0.268}(OH)_2(AR337)_{0.197}(BP\text{-}4)_{0.071}\cdot 0.61H_2O$
LDH-100	21.27	3.01	5.192	26.84	2.553	100	$Zn_{0.719}Al_{0.281}(OH)_2(AR337)_{0.281}\cdot 0.72H_2O$

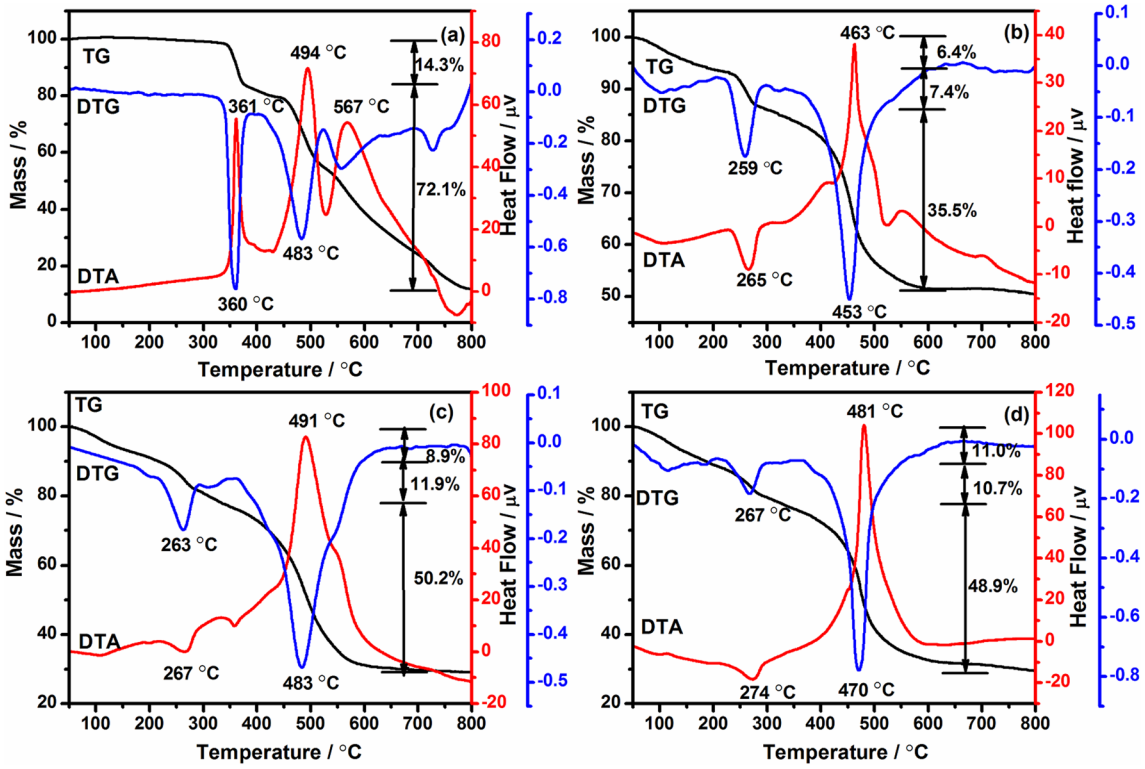

Figure 6. TG−DTG−DTA curves of (a) AR337, (b) LDH-0, (c) LDH-100, and (d) LDH-20.

anions. The mass loss of this stage is about 35.5%, which is less than the value of 45.8% calculated from the structural formula of LDH-0, suggesting that residue exists. As shown in Figure 6c, the TG−DTG−DTA curves of LDH-100 are very different from those of AR337. There are three mass loss steps in its TG curve. The first mass loss stage from 50 to 200 °C with a mass loss of 8.9% is attributed to the removal of adsorbed water and interlayer water. The second mass loss step emerged at 200−320 °C and is assigned to the dehydroxylation of the LDH layers, showing a mass loss of 11.9%. The third mass loss step is between 320 and 800 °C and is caused by the oxidative thermal decomposition of AR337 anions in the interlayer galleries of ZnAl−LDHs with an exothermic peak centered at 491 °C in the DTA curve. The mass loss of this stage is about 50.2%, which accords well with the value of 53.1% calculated from the structural formula of LDH-100. The mass loss in the range of 320−380 °C is about 4.2%, which is considerably smaller than that of AR337, suggesting that the thermal stability of AR337 is improved by intercalating into the interlayer of LDH. In comparison with LDH-0, the temperature of the exothermic peak for LDH-100 is much higher, indicating that the intercalated AR337 anion is more stable than the intercalated BP-4 anion. The TG−DTG−DTA curves of LDH-20 (Figure 6d) are similar to those of LDH-0 and LDH-100. The first mass loss step from 50 to 200 °C and the second mass loss step from 200 to 320 °C are attributed to the removal of adsorbed water and interlayer water and the dehydroxylation of the LDH layers, respectively. The third mass loss step from 320 to 800 °C and the exothermic peak centered at 481 °C indicate the oxidative thermal decomposition of the AR337 and BP-4 anions in the interlayer galleries of ZnAl−LDHs. This step shows a mass loss of 48.9%, which is well in accordance with the content of AR337 and BP-4 (47.8%) calculated from the structural formula of LDH-20. The results above illustrate that the oxidative thermal decomposition temperature for AR337 anions in the interlayer galleries of ZnAl−LDHs is much higher than that of the pristine AR337. Therefore, the intercalation into the interlayer room of LDH can enhance the thermal stability of AR337.

The thermal stability of the AR337 and LDH-100 was further investigated by FT−IR analysis. The samples were heated in an oven at 300 and 360 °C for 15 min, respectively. The mass loss percent of the samples after heating are listed in Table S1 (Supporting Information), and the FT−IR spectra of the samples before and after heating are shown in Figure S1 (Supporting Information). Both spectra of AR337 and LDH-100 show little change after heating at 300 °C, suggesting that they can stand for the heating temperature of 300 °C. However,

both of them underwent considerable decomposition after heating at 360 °C, as significant changes are observed in their spectra. AR337 shows a mass loss of 20.99% after heating at 360 °C. As the mass loss of LDH-100 after heating at 300 °C is mainly due to the removal of water and dehydroxylation of the LDH layers, the mass loss percent for AR337 anions in LDH-100 by heating at 360 °C is about 7%, which occupies about 14% of the AR337 anions in the interlayer of LDH-100. Hence, the intercalation into the interlayer of LDH can improve the stability of AR337 and slow down the thermal decomposition speed of AR337.

3.4. UV−Vis Spectra of Hybrid Pigments. Figure 7 shows the UV−visible absorption spectra of water solution of

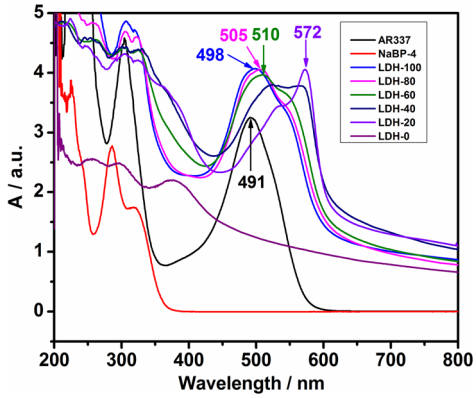

Figure 7. UV−vis spectra of water solution of AR337, NaBP-4, and ZnAl−AB−LDHs dispersed in ethanol.

AR337, NaBP-4, and ZnAl−AB−LDHs dispersed in ethanol. In comparison with the spectrum of AR337, the absorption spectrum of LDH-100 shows red shift in the visible region between 400 and 600 nm (shift from 491 to 498 nm). It is generally admitted that the absorption shifts of dye molecules are caused by polarity effects arising from the interactions between the dye molecules and their neighboring molecules. Dye molecules usually form H-type or J-type aggregates, which are characterized by a blue shift or red shift in the absorption band with respect to the monomer.[28,36−38] Hence, the red shift of absorption band of AR337 indicates that the intercalated AR337 anions formed J-type aggregates favored by the confinement of AR337 anions within the restricted space of the LDH interlayer region. The spectra of ZnAl−AB−LDHs in the visible region gradually shift to longer wavelengths as the amount of BP-4 anions increases. The maximum absorption peaks of LDH-40 and LDH-20 appearing at about 572 nm in the region of 550−650 nm are attributed to AR337 anions because LDH-0 shows no absorption peak in the region of 400−800 nm. The maximum absorption peak of LDH-20 is red-shifted about 74 nm in comparison with LDH-100, indicating that there are guest−guest interactions between AR337 anions and BP-4 anions favored by the restrict of LDH sheets. ZnAl−AS−LDH shows a maximum absorption centered at 530 nm (Figure S2, Supporting Information), which is red-shifted about 32 nm in comparison with LDH-100. Compared with AR337, the maximum absorption peak of ZnAl−ASS−LDH shows a red shift of merely 3 nm (Figure S2, Supporting Information), indicating that the interactions between AR337 anions and SDS anions are very weak. These results suggest that the significant red shift for LDH-20 may arise from the $\pi-\pi$ interactions between the benzene rings of AR337 and BP-4 anions. The interactions between AR337 anions and BP-4 anions were further confirmed by the UV−vis absorption spectra of the mixture solution of AR337 and NaBP-4, which were displayed in Figure S2 (Supporting Information). The spectrum of AR337 shows a maximum absorption at 491 nm, and NaBP-4 shows no absorption in the region of 400−800 nm. However, the mixture solution of AR337 and NaBP-4 exhibits a maximum absorption at 509 nm, which is red-shifted for about 18 nm in comparison with AR337, suggesting that interactions occur between AR337 and BP-4 anions that affect the absorption wavelength of AR337. Therefore, the guest−guest interactions between AR337 anions and BP-4 anions have a tremendous influence on the optical property of ZnAl−AB−LDHs.

3.5. Color Analysis. The digital photos of powdered ZnAl−AB−LDHs are shown in Figure 8A, and the color standard for

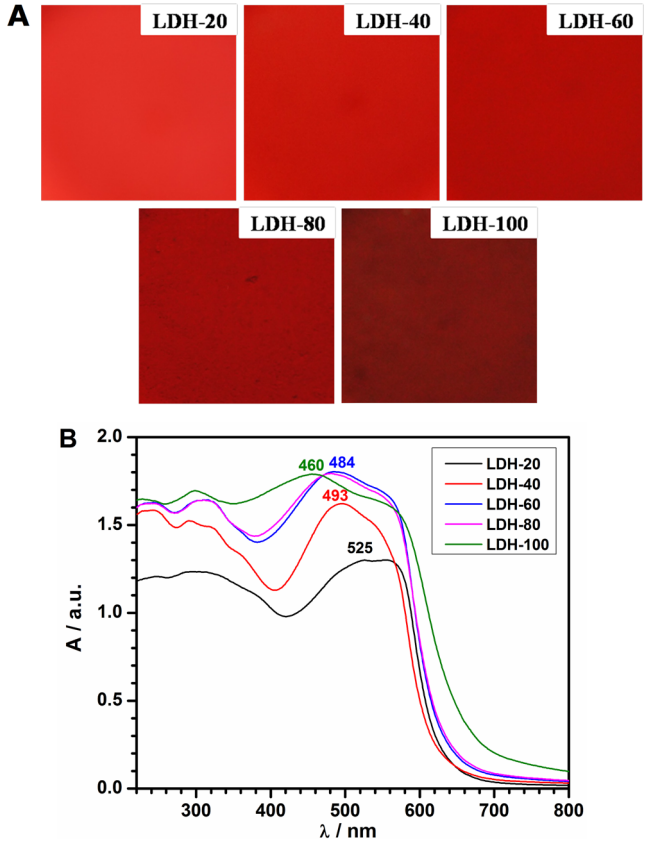

Figure 8. (A) Digital photos and (B) diffuse reflectance spectra of powdered ZnAl−AB−LDHs.

each sample is displayed in Figure S3 (Supporting Information). The color of the hybrid pigments gradually changes to deep with the increase of AR337 content. The color of the hybrid is pink when the molar percentage of AR337 is 20% and then changes to bright red when the molar percentage of AR337 increases to 40%. As the content of AR337 further increases, the color of the hybrid pigment varies to deep red and dark red. Figure 8B shows the diffuse reflectance spectra of the powdered ZnAl−AB−LDHs. The absorption intensity of ZnAl−AB−LDHs in the range of 400−650 nm increases as the content of AR337 increases at first and then remains nearly unchanged when the content of AR337 exceeds 60%. This trend is in accordance with the color change trend of the sample. The maximum absorption peak of ZnAl−AB−LDHs

gradually shifts from 525 to 460 nm when the molar percent of AR337 increases from 20 to 100%, which may result from the guest−guest interactions between guest anions in the interlayer. As shown in Figure S4 (Supporting Information), the hybrid pigment can be used as filler to prepare colored coating.

Figure 9 reveals the L*a*b* values of ZnAl−AB−LDHs hybrid pigments. The L*, a*, and b* values stand for the level

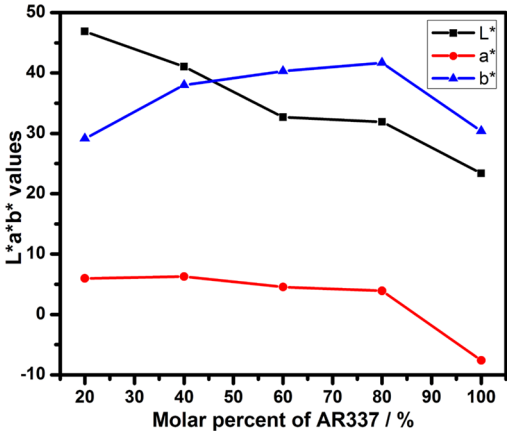

Figure 9. L*a*b* values of LDHs prepared with different molar percentages of AR337.

of lightness or darkness, redness or greenness, and yellowness or blueness, respectively. One sees that the L*a*b* values change with the increase of molar percentage of AR337. The L* value gradually decreases, indicating that the lightness of the hybrid pigment gradually decreases as the content of AR337 increases. The a* value remains positive but slightly decreases as the molar percentage of AR337 increases from 20 to 80%, suggesting that the color hue of the pigment is red but the redness decreases a little. However, the a* value varies from positive to negative when the molar percentage of AR337 increases to 100%, which suggests that the color hue of the pigments transfers from red to green. The b* value increases with the increase of AR337 content until the molar percentage of AR337 reaches 80%, and then it decreases, suggesting that the yellowness of the pigment first increases and then decreases.

3.6. Photostability Analysis. The photostability of the hybrid pigment was tested in a UV accelerating photoaging instrument, and the obtained results are shown in Figure 10A. The ΔE values of the samples become larger as the photoaging time increases, suggesting that the photooxidation degree of the samples increases. The ΔE value of PM increases from 5 to 15 when the photoaging time increases from 5 to 50 min, indicating that the physical mixture underwent considerable photooxidation. The ΔE values of MLDH-100 are smaller than those of PM after irradiation for the same time, suggesting that the photostability of MLDH-100 is superior to PM. The XRD patterns of PM in Figure S5 (Supporting Information) confirm that only a little of AR337 was intercalated into ZnAl−LDH. Therefore, the intercalation into the interlayer galleries of ZnAl−LDH can improve the photostability of AR337 due to the protection effects of LDHs host layers. The ΔE values of LDH-20, MLDH-40, MLDH-60, and MLDH-80 are much smaller than those of MLDH-100 after irradiation for the same times, and they are in the sequence of LDH-20 < MLDH-40 < MLDH-60 < MLDH-80, indicating that the photostability of the samples is in the sequence of LDH-20 > MLDH-40 > MLDH-60 > MLDH-80 > MLDH-100. It can be concluded that the co-intercalation of AR337 and BP-4 into the interlayer of ZnAl−LDHs can improve the photostability of AR337, and a higher degree of the improvement is obtained as the content of BP-4 increases.

The UV−vis spectra and the changes in the absorption of the tested samples after irradiation are illustrated in Figure S6 (Supporting Information) and Figure 10B, respectively. These results are in accordance with the photostability of samples revealed by the ΔE values. The photostability of PM could be considered to be the lowest, and only 76.7% of absorption was maintained after 50 min of irradiation. MLDH-100, MLDH-80, MLDH-60, MLDH-40, and LDH-20 maintain 80.3, 83.8, 86.9, 90.3, and 94.3% of absorption, respectively. Hence, the co-intercalation of AR337 with BP-4 can bring about a stabilization effect for AR337 because the BP-4 UV absorbent can absorb ultraviolet rays, which could result in the photo degradation of

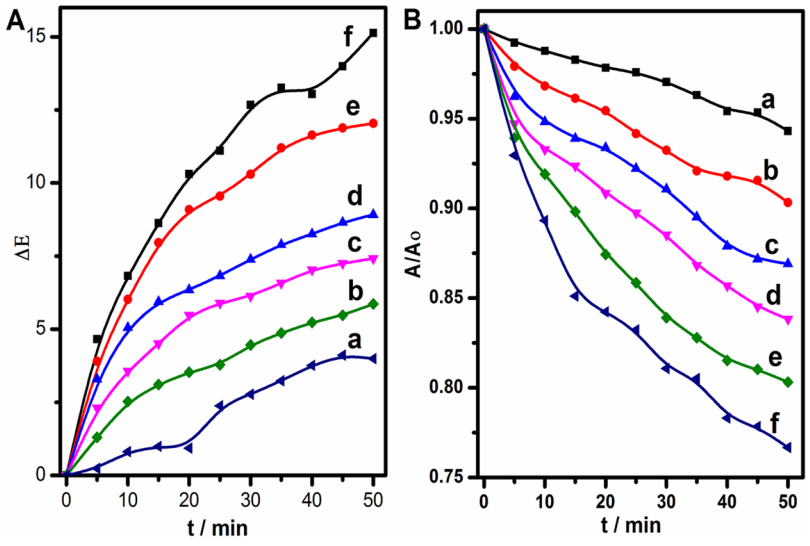

Figure 10. (A) ΔE values and (B) changes in absorption of the (a) LDH-20, (b) MLDH-40, (c) MLDH-60, (d) MLDH-80, (e) MLDH-100, and (f) PM after UV aging for different times.

AR337. Therefore, the co-intercalation of AR337 and BP-4 into the interlayer of ZnAl–LDH can effectively enhance the photostability of AR337.

4. CONCLUSIONS

A series of AR337 and BP-4 anions co-intercalated ZnAl–LDHs have been successfully prepared by coprecipitation method. The characterization results suggest that there are host–guest interactions between the LDH host layers and interlayer guest anions in ZnAl–AB–LDHs. The intercalation of the AR337 anions into the interlayer space of ZnAl–LDHs can enhance its thermo- and photostability as a result of the protections offered by the LDHs layers. The co-intercalation of AR337 with BP-4 into the interlayer room of LDH can further enhance the photostability of AR337 due to the excellent UV absorption ability of BP-4 and the incorporation of BP-4 can also tune the color of the hybrid pigment. This kind of hybrid pigment with excellent thermo- and photostability would have potential applications in the fields of plastics and coatings. This strategy can be easily extended to prepare other colored organic–inorganic hybrid pigments with improved thermo- and photostability.

■ ASSOCIATED CONTENT

Supporting Information

Preparation of coating, additional table, color standard, FT–IR spectra, UV–vis spectra, digital photo of coating, and XRD patterns. This material is available free of charge via the Internet at http://pubs.acs.org.

■ AUTHOR INFORMATION

Corresponding Authors

*E-mail: tangpg@mail.buct.edu.cn. Tel.: +86–10–64451007. Fax: +86–10–64425385.
*E-mail: yanglan@mail.buct.edu.cn.

Notes

The authors declare no competing financial interest.

■ ACKNOWLEDGMENTS

This work was supported by the National Natural Science Foundation of China (Grants 21036001 and 21206005), the Fundamental Research Funds for the Central Universities (YS1406), and the State Key Laboratory of Chemical Resource Engineering.

■ REFERENCES

(1) Jesionowski, T.; Przybylska, A.; Kurc, B.; Ciesielczyk, F. Hybrid Pigments Preparation via Adsorption of C.I. Mordant Red 3 on Both Unmodified and Aminosilane–Functionalised Silica Supports. *Dyes Pigm.* **2011**, *89*, 127–136.
(2) Cao, L.; Fei, X.; Zhang, T.; Yu, L.; Gu, Y.; Zhang, B. Modification of C.I. Pigment Red 21 with Sepiolite and Lithopone in Its Preparation Process. *Ind. Eng. Chem. Res.* **2014**, *53*, 31–37.
(3) Thetford, D.; Chorlton, A. P.; Hardman, J. Synthesis and Properties of Some Polycyclic Barbiturate Pigments. *Dyes Pigm.* **2003**, *59*, 185–191.
(4) Sanchez, C.; Belleville, P.; Popall, M.; Nicole, L. Applications of Advanced Hybrid Organic–Inorganic Nanomaterials: From Laboratory to Market. *Chem. Soc. Rev.* **2011**, *40*, 696–753.
(5) Williams, G. R.; O'Hare, D. Towards Understanding, Control, and Application of Layered Double Hydroxide Chemistry. *J. Mater. Chem.* **2006**, *16*, 3065–3074.
(6) Wang, Q.; O'Hare, D. Recent Advances in the Synthesis and Application of Layered Double Hydroxide (LDH) Nanosheets. *Chem. Rev.* **2012**, *112*, 4124–4155.
(7) Feng, Y.; Jiang, Y.; Huang, Q.; Chen, S.; Zhang, F.; Tang, P.; Li, D. High Antioxidative Performance of Layered Double Hydroxides/Polypropylene Composite with Intercalation of Low–Molecular–Weight Phenolic Antioxidant. *Ind. Eng. Chem. Res.* **2014**, *53*, 2287–2292.
(8) Yan, D.; Lu, J.; Ma, J.; Qin, S.; Wei, M.; Evans, D. G.; Duan, X. Layered Host–Guest Materials with Reversible Piezochromic Luminescence. *Angew. Chem., Int. Ed.* **2011**, *50*, 7037–7040.
(9) Crites, C. O. L.; Hallett-Tapley, G. L.; Frenette, M.; Gonzalez-Bejar, M.; Netto-Ferreira, J. C.; Scaiano, J. C. Insights into the Mechanism of Cumene Peroxidation Using Supported Gold and Silver Nanoparticles. *ACS Catal.* **2013**, *3*, 2062–2071.
(10) Cho, S.; Jang, J. W.; Kong, K. J.; Kim, E. S.; Lee, K. H.; Lee, J. S. Anion–Doped Mixed Metal Oxide Nanostructures Derived from Layered Double Hydroxide as Visible Light Photocatalysts. *Adv. Funct. Mater.* **2013**, *23*, 2348–2356.
(11) Gong, M.; Li, Y.; Wang, H.; Liang, Y.; Wu, J. Z.; Zhou, J.; Wang, J.; Regier, T.; Wei, F.; Dai, H. An Advanced Ni–Fe Layered Double Hydroxide Electrocatalyst for Water Oxidation. *J. Am. Chem. Soc.* **2013**, *135*, 8452–8455.
(12) Choi, S. J.; Choy, J. H. Layered Double Hydroxide Nanoparticles as Target-Specific Delivery Carriers: Uptake Mechanism and Toxicity. *Nanomedicine* **2011**, *6*, 803–814.
(13) Park, D. H.; Hwang, S. J.; Oh, J. M.; Yang, J. H.; Choy, J. H. Polymer–Inorganic Supramolecular Nanohybrids for Red, White, Green, and Blue Applications. *Prog. Polym. Sci.* **2013**, *38*, 1442–1486.
(14) Othman, M. A.; Zahid, W. M.; Abasaeed, A. E. Selectivity of Layered Double Hydroxides and Their Derivative Mixed Metal Oxides as Sorbents of Hydrogen Sulfide. *J. Hazard. Mater.* **2013**, *254*, 221–227.
(15) Theiss, F. L.; Couperthwaite, S. J.; Ayoko, G. A.; Frost, R. L. A Review of the Removal of Anions and Oxyanions of the Halogen Elements from Aqueous Solution by Layered Double Hydroxides. *J. Colloid Interface Sci.* **2014**, *417*, 356–368.
(16) Wen, T.; Wu, X.; Tan, X.; Wang, X.; Xu, A. One-Pot Synthesis of Water-Swellable Mg–Al Layered Double Hydroxides and Graphene Oxide Nanocomposites for Efficient Removal of As(V) from Aqueous Solutions. *ACS Appl. Mater. Interfaces* **2013**, *5*, 3304–3311.
(17) Liang, J.; Ma, R.; Iyi, N.; Ebina, Y.; Takada, K.; Sasaki, T. Topochemical Synthesis, Anion Exchange, and Exfoliation of Co–Ni Layered Double Hydroxides: A Route to Positively Charged Co–Ni Hydroxide Nanosheets with Tunable Composition. *Chem. Mater.* **2010**, *22*, 371–378.
(18) Chen, L.; Sun, K.; Li, P.; Fan, X.; Sun, J.; Ai, S. DNA-Enhanced Peroxidase-like Activity of Layered Double Hydroxide Nanosheets and Applications in H_2O_2 and Glucose Sensing. *Nanoscale* **2013**, *5*, 10982–10988.
(19) Shi, W.; He, S.; Wei, M.; Evans, D. G.; Duan, X. Optical pH Sensor with Rapid Response Based on a Fluorescein-Intercalated Layered Double Hydroxide. *Adv. Funct. Mater.* **2010**, *20*, 3856–3863.
(20) Leroux, F.; Illaik, A.; Stimpfling, T.; Troutier-Thuilliez, A. L.; Fleutot, S.; Martinez, H.; Cellier, J.; Verney, V. Percolation Network of Organo-Modified Layered Double Hydroxide Platelets into Polystyrene Showing Enhanced Rheological and Dielectric Behavior. *J. Mater. Chem.* **2010**, *20*, 9484–9494.
(21) Kang, N. J.; Wang, D. Y.; Kutlu, B.; Zhao, P. C.; Leuteritz, A.; Wagenknecht, U.; Heinrich, G. A New Approach to Reducing the Flammability of Layered Double Hydroxide (LDH)-Based Polymer Composites: Preparation and Characterization of Dye Structure-Intercalated LDH and Its Effect on the Flammability of Polypropylene-Grafted Maleic Anhydride/d-LDH Composites. *ACS Appl. Mater. Interfaces* **2013**, *5*, 8991–8997.
(22) Coelho, C.; Hennous, M.; Verney, V.; Leroux, F. Functionalisation of Polybutylene Succinate Nanocomposites: From Structure to Reinforcement of UV-Absorbing and Mechanical Properties. *RSC Adv.* **2012**, *2*, 5430–5438.

(23) Latterini, L.; Nocchetti, M.; Aloisi, G. G.; Costantino, U.; Elisei, F. Organized Chromophores in Layered Inorganic Matrices. *Inorg. Chim. Acta* **2007**, *360*, 728−740.
(24) Tang, P.; Feng, Y.; Li, D. Facile Synthesis of Multicolor Organic−Inorganic Hybrid Pigments Based on Layered Double Hydroxides. *Dyes Pigm.* **2014**, *104*, 131−136.
(25) Bauer, J.; Behrens, P.; Speckbacher, M.; Langhals, H. Composites of Perylene Chromophores and Layered Double Hydroxides: Direct Synthesis, Characterization, and Photo- and Chemical Stability. *Adv. Funct. Mater.* **2003**, *13*, 241−248.
(26) Chakraborty, C.; Dana, K.; Malik, S. Intercalation of Perylenediimide Dye into LDH Clays: Enhancement of Photostability. *J. Phys. Chem. C* **2010**, *115*, 1996−2004.
(27) Marangoni, R.; Bouhent, M.; Taviot−Guého, C.; Wypych, F.; Leroux, F. Zn_2Al Layered Double Hydroxides Intercalated and Adsorbed with Anionic Blue Dyes: A Physico-Chemical Characterization. *J. Colloid Interface Sci.* **2009**, *333*, 120−127.
(28) Marangoni, R.; Taviot-Guého, C.; Illaik, A.; Wypych, F.; Leroux, F. Organic Inorganic Dye Filler for Polymer: Blue-Coloured Layered Double Hydroxides into Polystyrene. *J. Colloid Interface Sci.* **2008**, *326*, 366−373.
(29) Tang, P.; Deng, F.; Feng, Y.; Li, D. Mordant Yellow 3 Anions Intercalated Layered Double Hydroxides: Preparation, Thermo- and Photostability. *Ind. Eng. Chem. Res.* **2012**, *51*, 10542−10545.
(30) Guo, X.; Xu, S.; Zhao, L.; Lu, W.; Zhang, F.; Evans, D. G.; Duan, X. One-Step Hydrothermal Crystallization of a Layered Double Hydroxide/Alumina Bilayer Film on Aluminum and Its Corrosion Resistance Properties. *Langmuir* **2009**, *25*, 9894−9897.
(31) Mandal, S.; Tichit, D.; Lerner, D. A.; Marcotte, N. Azoic Dye Hosted in Layered Double Hydroxide: Physicochemical Characterization of the Intercalated Materials. *Langmuir* **2009**, *25*, 10980−10986.
(32) Zhang, J.; Su, H.; Zhou, J.; Qian, G.; Xu, Z.; Xi, Y.; Xu, Y.; Theiss, F. L.; Frost, R. Mid- and Near-Infrared Spectroscopic Investigation of Homogeneous Cation Distribution in $Mg_xZn_yAl_{(x+y)/2}$−Layered Double Hydroxide (LDH). *J. Colloid Interface Sci.* **2013**, *411*, 240−246.
(33) Chen, C.; Yee, L. K.; Gong, H.; Zhang, Y.; Xu, R. A Facile Synthesis of Strong Near Infrared Fluorescent Layered Double Hydroxide Nanovehicles with an Anticancer Drug for Tumor Optical Imaging and Therapy. *Nanoscale* **2013**, *5*, 4314−4320.
(34) Sun, Z.; Jin, L.; Shi, W.; Wei, M.; Duan, X. Preparation of an Anion Dye Intercalated into Layered Double Hydroxides and Its Controllable Luminescence Properties. *Chem. Eng. J.* **2010**, *161*, 293−300.
(35) Wang, H.; Xiang, X.; Li, F. Hybrid ZnAl−LDH/CNTs Nanocomposites: Noncovalent Assembly and Enhanced Photodegradation Performance. *AlChE J.* **2010**, *56*, 768−778.
(36) Hirano, Y.; Tateno, S.; Ozaki, Y. Thermal Behavior of J-Aggregates in Mixed Langmuir−Blodgett Films Composed of Merocyanine Dye and Deuterated Arachidic Acid Investigated by UV−Visible and Infrared Absorption Spectroscopy. *Langmuir* **2007**, *23*, 7003−7013.
(37) Berlepsch, H. v.; Ludwig, K.; Bottcher, C. Pinacyanol Chloride Forms Mesoscopic H- and J-aggregates in Aqueous Solution—A Spectroscopic and Cryo-Transmission Electron Microscopy Study. *Phys. Chem. Chem. Phys.* **2014**, *16*, 10659−10668.
(38) Kinashi, K.; Lee, K. P.; Matsumoto, S.; Ishida, K.; Ueda, Y. Alkyl Substituent Effects on J- or H-Aggregate Formation of Bisazomethine Dyes. *Dyes Pigm.* **2012**, *92*, 783−788.